TRANSLAMINAR FRACTURE TOUGHNESS CHARACTERISATION OF CARBON FIBRE REINFORCED THERMOPLASTIC COMPOSITES

M. A. A. Mohsin[1*], L. Iannucci[1] and E. Greenhalgh[1]

[1]Imperial College London, Department of Aeronautics, Imperial College London, Exhibition Road, London SW7 2AZ, United Kingdom
[1*]Email: m.mohsin14@imperial.ac.uk, Web Page: http://www.imperial.ac.uk

Keywords: lightweight vehicle design, high-performance composites, composite structures, fracture toughness

Abstract

The translaminar fracture toughness of carbon/thermoplastic T700/PA6.6 composite system was examined. The fracture toughness test was conducted using compact tension specimens of non-crimp fabric biaxial T700 carbon fibre reinforced PA6.6. The critical strain energies, G_{Ic}^{0}, required to initiate and propagate the crack through the specimen were found to be between $72-81kJ/m^2$ and $77-95kJ/m^2$ respectively. Two compact tension (CT) specimen configurations were validated though finite element modelling (FEM) using LS-DYNA® prior to the test.

Nomenclature

a	crack length (mm)
a_0	pre-crack length (mm)
C	compliance (mm/kN)
d	displacement (mm)
E	Young's modulus (GPa)
G_{Ic}	fracture toughness (J/m^2)
h	height (mm)
K_{Ic}	stress intensity factor
P	load (kN)
P_c	critical load (kN)
t	thickness (mm)
w	width (mm)

1. Introduction

1.1. Background

There has been a growing interest in thermoplastic (TP) composites in the automotive industry due to their superior mechanical performance over thermosetting (TS) composites. Despite weighing less than 50% of steel, TP composites exhibit improvements payload and strength. Hence, the characterisation of their failure resistance, such as fracture, will contribute to composite materials database. This allows for better prediction of the materials behaviour under impact and crash and improve post-damage analysis.

Excerpt from ISBN 978-3-00-053387-7

The material system selected was a carbon/TP system (T700/PA6.6) with fibre volume fraction (FVF) of approximately 50% (supplied by THERMOCOMP [1]). The specimen was modelled using finite element (FE) solver LS-DYNA®, where the final dimensions of the CT specimen were determined when the only failure observed was fibre failure at the crack tip.

To date, the information on the translaminar fracture toughness of TP composites is limited. Therefore, this study aims to fill the gap and report the tensile translaminar fracture toughness associated with TP composites.

1.2. Non-crimp fabric (NCF) composites

The idea of developing non-crimp fabric (NCF) reinforcement instead of conventional textiles began in 1982 [2]. It was designed as an alternative and more cost effective solution to conventional textiles [2]. The manufacturing process of NCF composites involve highly automated techniques which include stitching, weaving, braiding and knitting [3]. Typical production techniques include bi-, tri- and quadri-axial fabrics of glass or carbon fibre using aramid warp knitting yarns. In this study, the NCF biaxial carbon fibres are utilised.

2. Translaminar fracture toughness

Unlike metals, the failure mode of composites material system is a complex multi-stage process. A failure of a composite structure may begin in a particular mode, but its propagation and final failure modes could be completely different. Fracture initiation and propagation are regarded as the final failure stage of laminated composite structures [4]. Hence, understanding the fracture propagation mechanism and associated translaminar fracture toughness is vital. Some of these failure modes include delamination, intralaminar and translaminar fracture. In contrast with delamination, translaminar fracture has not received much attention from the scientific community until recently.

The translaminar failure mode is a fibre-dominated toughness which plays an important role in evaluating the damage tolerance and response of a composite structure. CT configurations (depicted in Fig. 1) are some of the most commonly used arrangements in the characterisation of translaminar fracture toughness measurement of composites. Nonetheless, largely for carbon/TS carbon/epoxy [4]–[8].

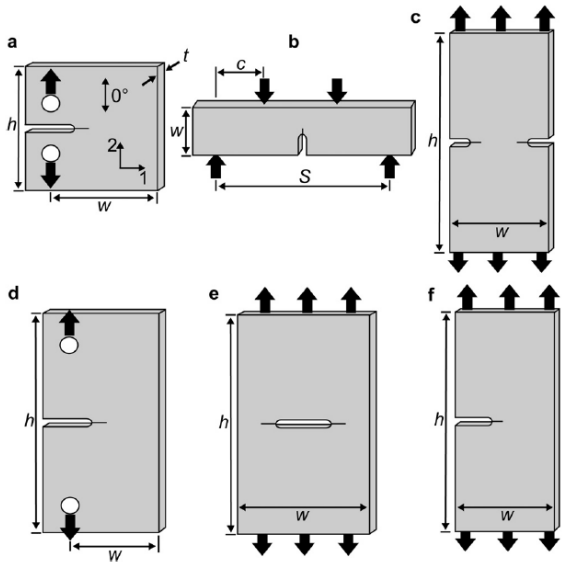

Figure 1. Some of the most common configurations used to characterise translaminar fracture toughness: (a) CT, (b) four-point bend, (c) double edge notched tension, (d) extended compact tension, (e) centre-notched tension and (f) single edge notched tension

Excerpt from ISBN 978-3-00-053387-7

3. Experimental method and data reduction

The use of CT specimens, in particular, has gained popularity in the literature as it promotes a more stable crack propagation than some other configurations. One of the most common problems in determining the right geometry and dimension of CT is compression failure at the back edge of the specimen, FM_1, shown in Fig. 2.

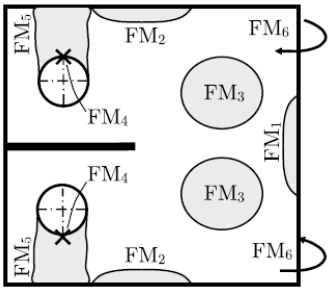

Figure 2. The six undesirable failure mechanisms commonly associated with CT specimen, reported by Blanco et al. [9]

The work done in the characterisation of translaminar fracture toughness of FRPs has largely revolved around TS composites systems [5], [7], [8] and there has not been much done to look into TP composites.

3.1. Numerical modelling of CT test

Prior to deciding the CT configuration of the T700/PA6.6, numerical validation using FEM was performed. The mechanical properties of the T700/PA6.6, which were input into the FE model (Fig. 4), were obtained from tensile [10], compressive [11], in-plane shear [12] and interlaminar tests [13], summarised in Table 1. In LS-DYNA®, these values were used to populate the material card representing the laminate. Fig. 5 shows the stress-strain curves obtained from the tensile and in-plane tests.

Table 1. Summary of the mechanical properties from characterisation of tensile and compressive properties of the materials tested and used for comparison

Material System	Tensile		In-plane Shear		Compression		Interlaminar Shear Strength (MPa)
	Modulus (GPa)	Strength (MPa)	Modulus (GPa)	Strength (MPa)	Modulus (GPa)	Strength (MPa)	
T700/PA6.6[a]	64.8	918	3.17	52.1	74.1	459	41.1

[a]*NCF biaxial T700/PA6.6 carbon/polyamide6.6 with FVF of approximately 50%*

The validation of the CT test allows the investigator to avoid the undesirable failure mechanisms as pictured in Fig. 2. In this case, the most common failure mechanism associated with the opted configuration of the CT specimen is the compressive failure at the back edge.

Two configurations of CT specimen were proposed (Fig. 3). Specimen A is the more conventional CT specimen configuration while specimen B is considered as the optimised configuration. The thickness, t, and height, h, for both specimens are 4mm and 60mm respectively. Specimen B was designed to capture a larger stable crack growth. The width, w, of the specimen B was extended to 66mm compared to 51mm in specimen A (Fig. 3). In this way, the pre-crack length, a_0 can be increased, from 26 to 36mm (Fig. 3), resulting in lower forces between the pins and the holes of the specimen due to the larger

Excerpt from ISBN 978-3-00-053387-7

moment induced to propagate the crack. Additionally, the semi-circular back edge of specimen B (Fig. 4a) allows for a more regular and gradual distribution of compressive stresses in comparison to the rectangular shape of specimen A (Fig. 4b). FE results confirmed that neither specimen would fail through the mechanisms described in Fig. 2.

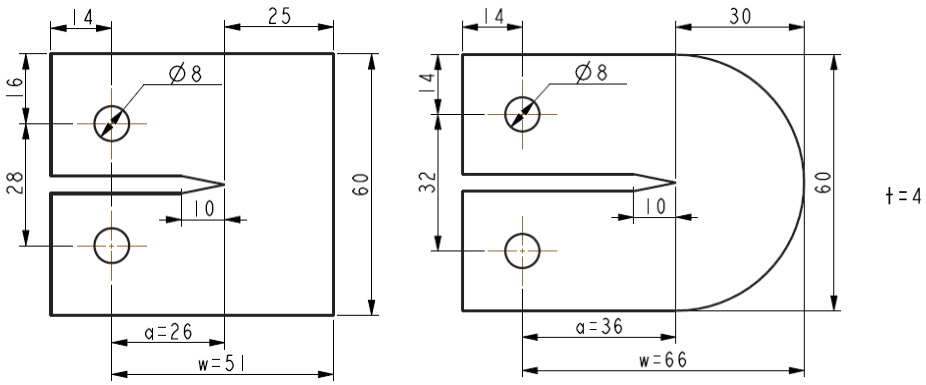

Figure 3. Dimensions of CT specimen configurations: specimen A (left) and specimen B (right)

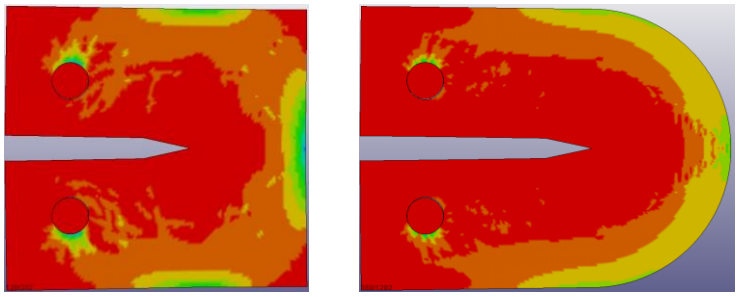

(a) (b)

Figure 4. The FE model illustrating the 3rd principal stresses (compressive stresses) of the two CT specimen configurations: (a) specimen A and (b) specimen B

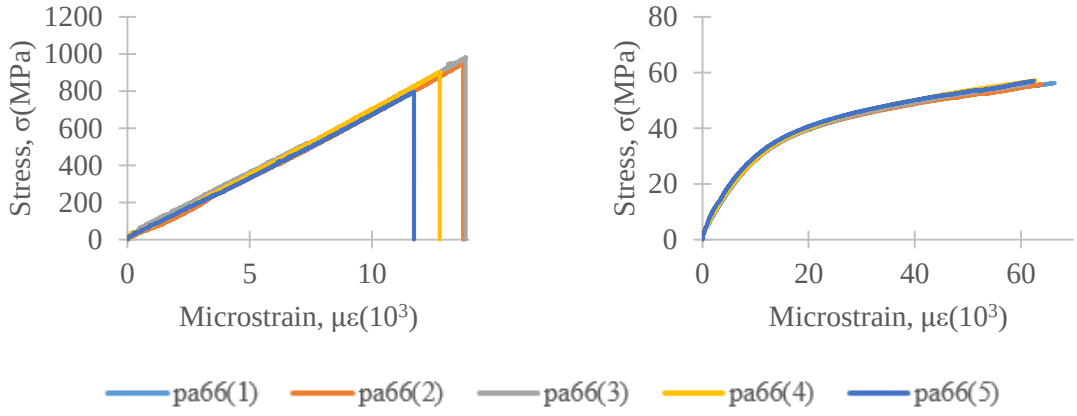

Figure 5. Stress-strain curves obtained from tensile (left) and shear tests (right)

Using the compliance calibration method [14], the critical strain energy release rate can be calculated using the rate of change of compliance, C, against crack length, a

Excerpt from ISBN 978-3-00-053387-7

$$G_{Ic} = \frac{P_c^2}{2t}\frac{dC}{da} \quad (1)$$

The compliance calibration method utilises the elastic compliance of the specimen at known crack lengths. This was acquired from the load-displacement plot generated from FEM.

3.2. Experimental setup

The CT specimens (Fig. 6) were cut using a waterjet cutter from the T700/PA6.6 laminated manufactured using compression moulding technique. The experimental setup of the CT test is as illustrated in Fig. 6. The displacement of the pins was measured using an optical strain camera. The loading rate was set to 1mm/min throughout the experiment.

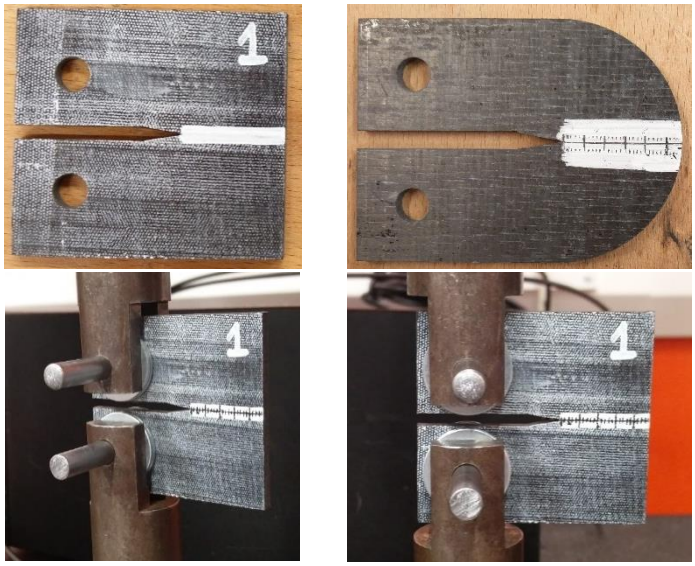

Figure 6. CT specimen A (top left) and specimen B (top right) of the T700/PA6.6 carbon fibre reinforced thermoplastic composite (CFRTP) and the CT test experimental setup (bottom left and right)

4. Results

The load-displacement curve for both CT specimen configurations is presented in Fig. 7. Both specimens demonstrated stick-slip crack growth of 1-2mm. However, specimen A was only able to achieve 5mm of total stable crack growth before failing in compression at its back edge. This was due to slight misalignment in the experimental setup. Nonetheless, specimen B exhibited considerable 23mm of stable crack growth.

Using the compliance calibration method, the compliance, C, for both specimen configurations were plotted against crack length, a (Fig. 8). The critical strain energy release rate, G_{Ic}^0, for initiation and propagation were calculated and plotted against the crack length, a, based on Eq. 1. The R-curves obtained from the selected method of data reduction are reported in Fig. 9.

Based on Fig. 9, it can be observed that the initiation and propagation G_{Ic}^0 for specimen A are 72.2 and $77.1 kJ/m^2$ (with coefficient of variance, $CV = 2.4\%$) respectively. Similarly, in relation to specimen B, the G_{Ic}^0 values measured for initiation and propagation are 81.1 and $95.3 kJ/m^2$ ($CV = 1.4\%$).

Excerpt from ISBN 978-3-00-053387-7

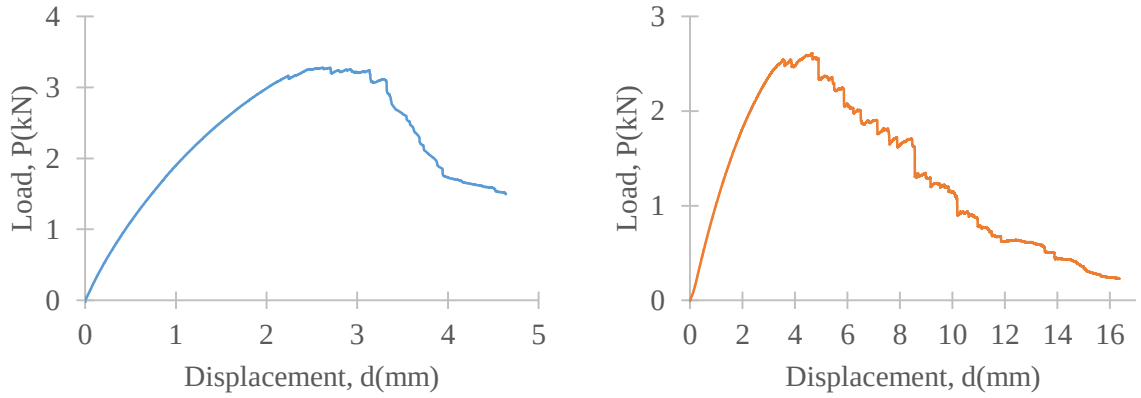

Figure 7. Load-displacement curve for CT specimen A (left) and specimen B (right)

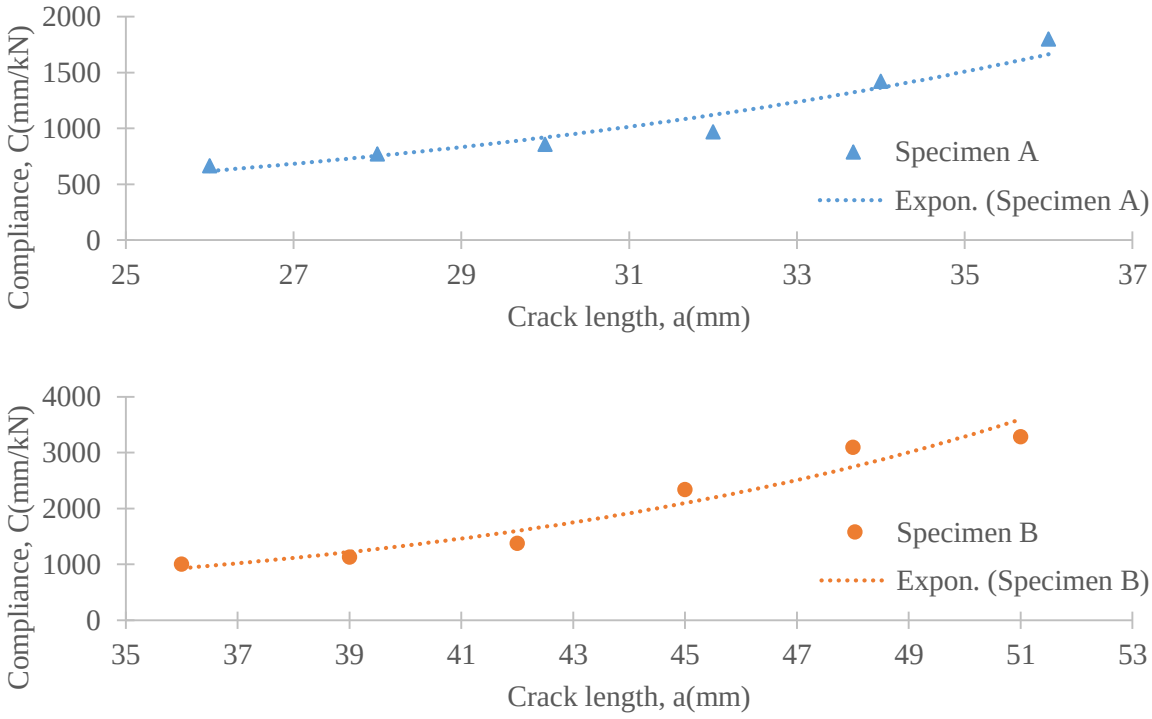

Figure 8. Curves of compliance against crack length for specimen A (top) and specimen B (bottom) obtained from FE through compliance calibration method

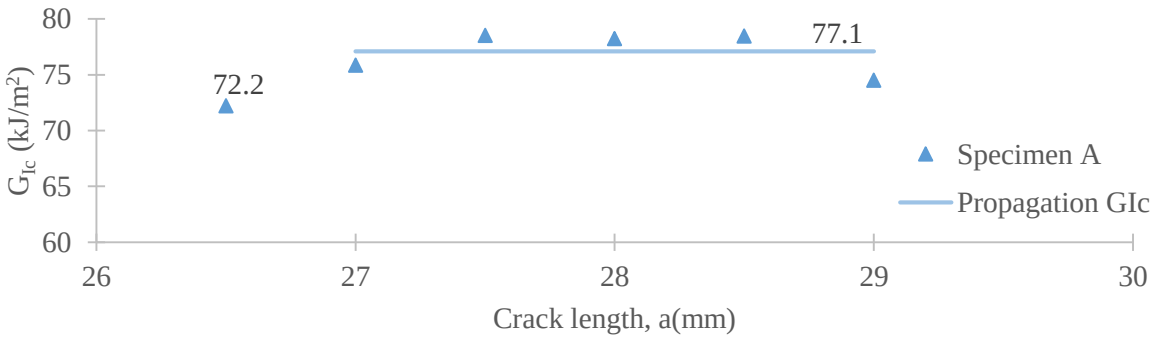

Excerpt from ISBN 978-3-00-053387-7

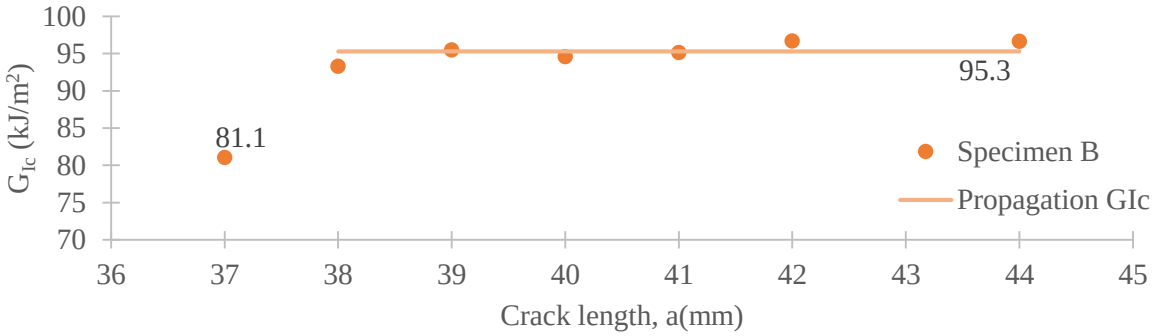

Figure 9. R-curves corresponding to critical strain energy release rates, G_{Ic}^{0} for specimen A (top) and specimen B (bottom), at varying crack lengths, a

5. Discussions

The mechanical properties of T700/PA6.6 such as tensile, compressive and shear were determined using standardised tests as per the ISO standards. These properties were utilised to establish the right configuration of the CT specimen, which was optimised through FE validation using LS-DYNA®.

Following the numerical modelling of the CT test, stable crack growth was achieved during the actual experiment. Nevertheless, due to a slight misalignment in the experimental setup, specimen A only achieved 5mm of stable crack growth. The optimised CT configuration, specimen B, on the other hand, exhibited a steady crack growth of 23mm. Therefore, since specimen B managed 23mm of steady crack growth, its G_{Ic}^{0} values are regarded as the more accurate representation of the tensile translaminar fracture toughness of the T700/PA6.6 composite system. Table 2 compares the G_{Ic}^{0} values of the T700/PA6.6 against some typical carbon fibre reinforced thermosetting (CFRTS) composite systems.

Table 2. Summary of experimental data gathered from the tensile translaminar fracture toughness characterisation of CFRTP and CFRTS systems

Study	Specimen configuration	Material system	$G_{Ic}^{0}(kJ/m^2)$	
			Initiation	Propagation
Mohsin et al. (this study)	CT	T700/PA6.6	81.1	95.3
Pinho et al. [5]	CT	T300/913	91.6	133.0
Catalanotti et al. [7]	CT	IM7/8552	97.8	133.3

Toughening mechanisms such as fibre bridging and fibre pull-out were detected in both specimens. The translaminar fracture toughness values for crack initiation and propagation were successfully quantified to be 81.1 and $95.3 kJ/m^2$ ($CV = 1.4\%$) in the 0° fibre direction.

6. Conclusions

The study conducted reports the methodology of characterising translaminar fracture toughness of TP composites, particularly NCF biaxial carbon/TP system T700/PA6.6. The T700/PA6.6 system showed similar fracture toughness values as some of the most common carbon/epoxy systems. Evidently, the optimised CT configuration, specimen B, was found to be the superior geometry in characterising the translaminar fracture toughness of the T700/PA6.6 composite in comparison to the more traditional CT configuration.
Considering the more rapid manufacturing process and the recyclability of CFRTP, it can be concluded that TP composites serve as the more practical and economical composite material solutions for the automotive industry.

Excerpt from ISBN 978-3-00-053387-7

Acknowledgments

The materials and support provided by THERMOCOMP partners for this research are highly appreciated.

References

[1] "UK-THERMOCOMP | CIC." [Online]. Available: http://the-cic.org.uk/uk-thermocomp. [Accessed: 05-Oct-2015].

[2] P. Steggall, "Developing multiaxial non-crimp reinforcements for the cost effective solution," in *Advanced Materials & Processes: Preparing for the New Millenium*, 1999, pp. 341–354.

[3] K. H. Leong, S. Ramakrishna, Z. M. Huang, and G. A. Bibo, "Potential of knitting for engineering composites - a review," *Compos. Part A Appl. Sci. Manuf.*, vol. 31, no. 3, pp. 197–220, 2000.

[4] N. Blanco, D. Trias, S. T. Pinho, and P. Robinson, "Intralaminar fracture toughness characterisation of woven composite laminates. Part II: Experimental characterisation," *Eng. Fract. Mech.*, vol. 131, pp. 361–370, 2014.

[5] S. T. Pinho, P. Robinson, and L. Iannucci, "Fracture toughness of the tensile and compressive fibre failure modes in laminated composites," *Compos. Sci. Technol.*, vol. 66, no. 13, pp. 2069–2079, 2006.

[6] M. J. Laffan, S. T. Pinho, and P. Robinson, "Mixed-mode translaminar fracture of CFRP: Failure analysis and fractography," *Compos. Struct.*, vol. 95, pp. 135–141, 2013.

[7] G. Catalanotti, P. P. Camanho, J. Xavier, C. G. Davila, and A. T. Marques, "Measurement of resistance curves in the longitudinal failure of composites using digital image correlation," *Compos. Sci. Technol.*, vol. 70, no. 13, pp. 1986–1993, 2010.

[8] M. J. Laffan, S. T. Pinho, P. Robinson, and A. J. McMillan, "Translaminar fracture toughness: The critical notch tip radius of 0° plies in CFRP," *Compos. Sci. Technol.*, vol. 72, no. 1, pp. 97–102, 2011.

[9] N. Blanco, D. Trias, S. T. Pinho, and P. Robinson, "Intralaminar fracture toughness characterisation of woven composite laminates. Part I: Design and analysis of a compact tension (CT) specimen," *Eng. Fract. Mech.*, vol. 131, pp. 349–360, 2014.

[10] British Standards Institution, "BS EN ISO 527-4:1997 BS 2782-3: Method 326F:1997 Plastics - Determination of tensile properties," *British Standards*, vol. 1. pp. 527–1, 2009.

[11] British Standards Institution, "BS EN ISO 14126:1999 Fibre-reinforced plastic composites - Determination of compressive properties in the in-plane direction," *British Standards*, vol. 3. 1999.

[12] British Standards Institution, "BS EN ISO 14129:1998 Fibre-reinforced composites - Determination of the in-plane shear stress/strain response, including the in-plane shear modulus and strength by the ± 45°," *British Standards*. 1998.

[13] British Standards Institution, "BS EN ISO 14130:1998 Fibre reinforced plastic composites - Determination of apparent interlaminar shear strength by short-beam method," *British Standards*, vol. 3, no. 1108. pp. 1–9, 1998.

[14] M. J. Laffan, S. T. Pinho, P. Robinson, and L. Iannucci, "Measurement of the in situ ply fracture toughness associated with mode I fibre tensile failure in FRP. Part I: Data reduction," *Compos. Sci. Technol.*, vol. 70, no. 4, pp. 606–613, 2010.

Excerpt from ISBN 978-3-00-053387-7